Article

Investigation on the Suitability of Engelhard Titanium Silicate as a Support for Ni-Catalysts in the Methanation Reaction

Patrizia Frontera [1],*, Mariachiara Miceli [1], Francesco Mauriello [1], Pierantonio De Luca [2] and Anastasia Macario [3]

[1] Department of Civil, Energy, Environmental and Materials Engineering, Mediterranea University of Reggio Calabria, Via Graziella, Loc. Feo di Vito, 89122 Reggio Calabria, Italy; mariachiara.miceli@unirc.it (M.M.); francesco.mauriello@unirc.it (F.M.)

[2] Department of Mechanical, Energy and Management Engineering, University of Calabria, Via P. Bucci, 87036 Cosenza, Italy; p.deluca@unical.it

[3] Department of Environmental Engineering, University of Calabria, Via P. Bucci, 87036 Cosenza, Italy; macario@unical.it

* Correspondence: patrizia.frontera@unirc.it

Abstract: Methanation reaction of carbon dioxide is currently envisaged as a facile solution for the storage and transportation of low-grade energies, contributing at the same time to the mitigation of CO_2 emissions. In this work, a nickel catalyst impregnated onto a new support, Engelhard Titanium Silicates (ETS), is proposed, and its catalytic performance was tested toward the CO_2 methanation reaction. Two types of ETS material were investigated, ETS-4 and ETS-10, that differ from each other in the titanium content, with Si/Ti around 2 and 3% by weight, respectively. Catalysts, loaded with 5% of nickel, were tested in the CO_2 methanation reaction in the temperature range of 300–500 °C and were characterized by XRD, SEM–EDX, N_2 adsorption–desorption and H_2-TPR. Results showed an interesting catalytic activity of the Ni/ETS catalysts. Particularly, the best catalytic performances are showed by Ni/ETS-10: 68% CO_2 conversion and 98% CH_4 selectivity at T = 400 °C. The comparison of catalytic performance of Ni/ETS-10 with those obtained by other Ni-zeolites catalysts confirms that Ni/ETS-10 catalyst is a promising one for the CO_2 methanation reaction.

Keywords: methanation; carbon dioxide; nickel; titanium silicate

1. Introduction

The Power to Gas technology, based on the conversion of electricity to hydrogen via electrolysis, is regarded among the most environmentally sustainable approaches that could enable the chemical storage of energy [1]. However, hydrogen is not the appropriate medium for a storage application due to the significant compression (>100 bar) required to reach a moderate energy density. In contrast, the energy density of methane (CH_4) is three times higher than hydrogen and facilities for transport and storage are widespread. Indeed, the methane can be produced converting hydrogen (H_2) with carbon dioxide (CO_2) following the well-known reaction (1) and easily stored as a renewable energy source:

$$4H_2(g) + CO_2(g) \rightleftarrows CH_4(g) + 2H_2O(g)\ \Delta H° = -165\ kJ\ mol^{-1} \tag{1}$$
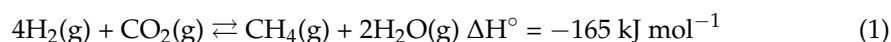
The carbon dioxide methanation reaction provides a solution for the storage and the transportation of low-grade energies. Moreover, it can potentially promote the abatement of polluting gas emissions since methane can be produced by simultaneously recycling carbon dioxide, CO_2 [1–5]. Indeed, carbon oxides are regarded the major pollutants in the atmosphere, and their decrement represents a pressing challenge necessary to detect and limit their harmful effects [6,7].

Catalytic methanation reactors are typically operated at temperatures between 200 °C and 550 °C and at pressures ranging from 1 to 100 bar, since CO_2 methanation is also a

strongly exothermic reaction and increasing the temperature is obviously unfavorable. However, it could be desirable to achieve higher conversions at the higher temperature when reagent gases (carbon monoxide, carbon dioxide and hydrogen) derive from other process, such as the reforming of hydrocarbon coal gasification processes, or came from the exit-streams of the solid oxide electrolyzer cells (SOECs).

Despite several metals, such as Ni, Ru, Rh and Co, being used as catalysts [8], Ni is considered the best one due to its low cost and catalytic performance.

Alongside the active metal, the support of this phase plays a fundamental role. The support can improve the dispersion of active components and tunes the surface structure of the catalysts; these effects can influence the adsorption characteristics of the species involved and, consequently, the reaction pathways [2,9]. Among the support tested, SiO_2-based materials, such as zeolites, used as supports for metal catalysts, exhibit peculiar features such as ordered structures, high surface area, large pore volume and affinity versus the CO_2 due to the intrinsic basicity of the support [10].

In the last years, different types of zeolites were used as metal supports to prepare active and stable catalysts [10]. Indeed, despite their massive utilization is mainly related to other specific applications, such as molecular sieves and adsorbent materials [11,12], their use in catalysis has manifold reasons: (i) the zeolite confinement effects (zeolite cages and channels intersections really act like nanoreactors, boosting catalysts' activity); (ii) the possibility to adapt their basicity or acidity by both cationic exchange with alkaline metals and post-synthesis treatments (e.g., dealumination); and (iii) their hydrothermal stability that can be improved by steaming treatments.

Recently, Bacariza et al. have reviewed several works about the use of zeolite-based catalysts for carbon dioxide methanation, showing the potentiality of zeolites as support catalysts in this reaction. The type of zeolites more investigated are Y, A, X and ZSM-5, which essentially differ for framework structure and aluminum content [13].

The Engelhard Titanosilicate (ETS) is a microporous material that presents a structure similar to that of inorganic microporous zeolites [14], composed of tetrahedral SiO_4^{4-} and octahedral TiO_6^{8-} units [15]. ETS-4 ($Na_9Si_{12}Ti_5O_{38}(OH)\cdot 12H_2O$) and ETS-10 ($M_2TiSi_5O_{13}$ H_2O with M = Na, K) both have a microporous structure but differ from each other in the Si/Ti ratio and in the pore size.

Few studies have employed the ETS material as catalyst support. In particular, in the dry reforming of methane, ETS-10 titanosilicate was proved to be an active and stable support for Ru species [16]. Philippou et al. [17] have used ETS-10 as Pt support in the hexane reforming, reporting that this material catalyzes the reaction with remarkably high selectivity. The mesoporous ETS-10 assembled Cu catalysts (named Cu/ETS-10-M) were also prepared and applied in the styrene functionalization reaction [18]. Santamaría and co-workers have investigated the use of Pt/ETS-10 catalyst for the selective oxidation of CO in the presence of H_2, CO_2 and H_2O concluding that the Pt–ETS-10 catalyst is active and selective in the above-mentioned reaction [19].

However, these materials, due to their porosity features, need more in-depth investigation to improve their application in the catalysis field.

In the present work, we investigated the suitability of ETS material as support for Ni catalyst in the methanation reaction. Ni/ETS-4 and Ni/ETS-10 catalysts have been prepared by impregnation method, characterized by different analytical techniques and tested in the methanation of carbon dioxide in the temperature range of 300–500 °C.

2. Results

2.1. Catalyst Characterization Results

X-ray diffraction patterns of synthesized ETS-4 (Figure 1, ETS-4 fresh) and ETS-10 (Figure 2, ETS-10 fresh) were found to be identical to the reference patterns reported in the literature (COD ID 4002324 and COD ID 7110493), confirming that the synthesized supports are pure ETS-4 and ETS-10.
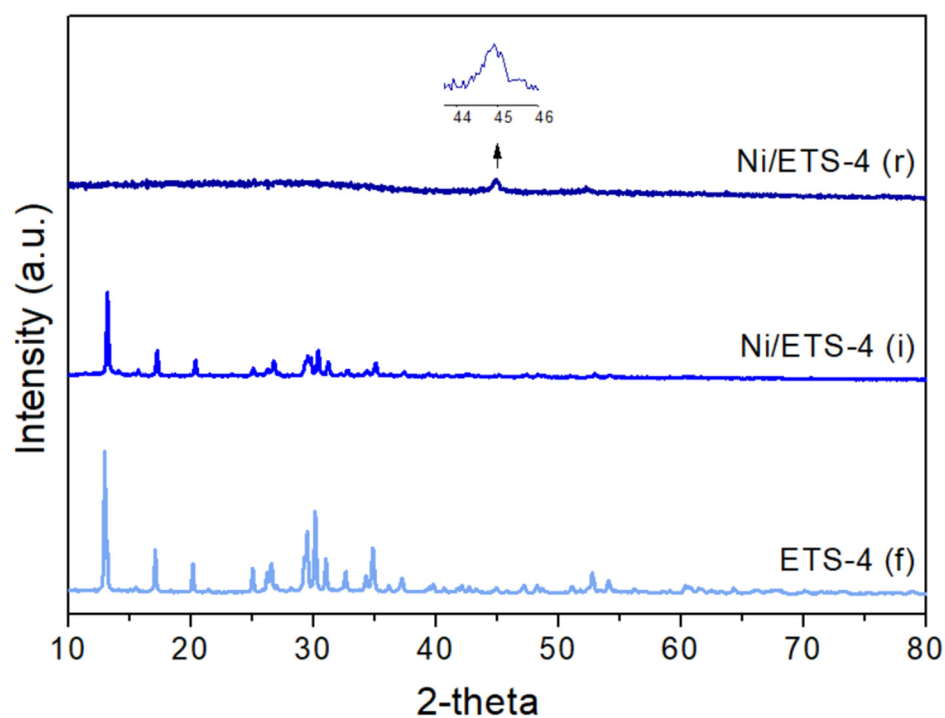
Figure 1. Diffraction pattern of fresh ETS-4 (f) and Ni/ETS-4 (i) after the impregnation treatment and Ni/ETS-4 (r) after the reduction treatment.
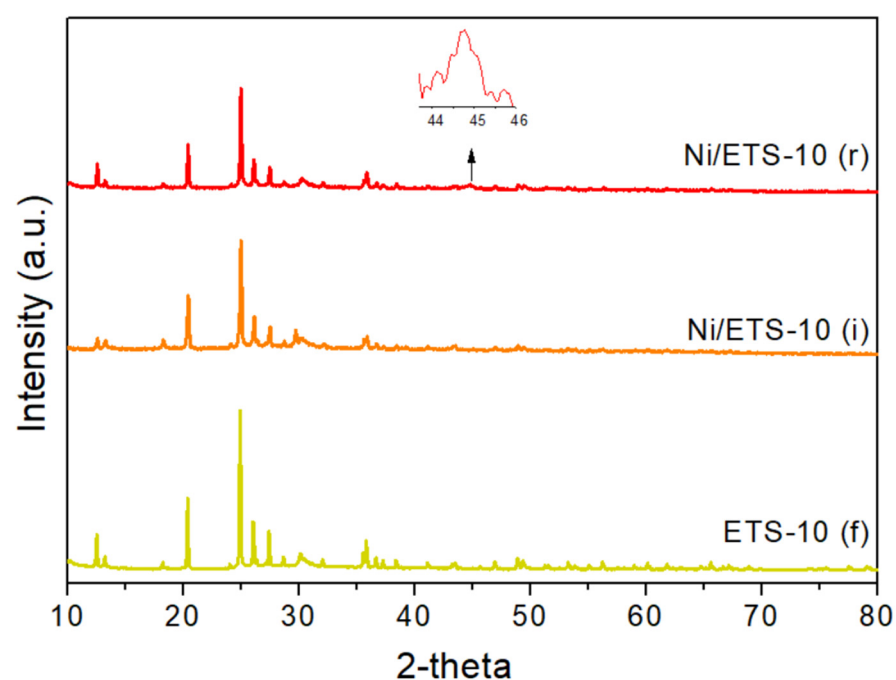

Figure 2. Diffraction pattern of fresh ETS-10 (f) and Ni/ETS-10 (i) after the impregnation treatment and Ni/ETS-10 (r) after the reduction treatment.

In order to check the support stability during the catalyst preparation, the XRD analysis was carried out after both the impregnation and reduction procedures (see Figures 1 and 2). Impregnation does not significantly modify the pattern of tested materials, but the reduction indeed destroyed the structure of ETS-4. In fact, in the related pattern (Figure 1, ETS-4 (r)), the only peak defined at around $2\theta = 44.6°$ corresponds to the metallic nickel (COD ID 9013004) (enlargement in Figure 1). In addition, in the reduced Ni/ETS-10 (Figure 2, ETS-10 (r)) the peak related to the metallic nickel (enlargement in

Figure 2) is detectable, and the broadness of this peak can be related to a very small particle size. The low thermal stability of ETS-4 is related to the hydrogen bonding between the extra framework water molecules and the framework oxygens, which leads to the formation of a vitreous amorphous phase [20].

Table 1 summarizes the main texture properties of supports and catalysts. The amount of deposited nickel is quite like the nominal content for both samples. The bare supports have microporous characteristics (the internal surface area is higher than the external one) and are characterized by a monomodal distribution in the range of micropores. The values of BET surface area of the as synthesized ETS are coherent to those reported in literature [21].

Table 1. Textural and Surface properties of bare support impregnated and catalyst samples.

Sample	Si/Ti [a]	Ni [a] [w/w%]	SBET [b] m^2/g	Sint [c] m^2/g	Sext [c] m^2/g	Vmic [c] cm^3/g	Vmes [d] cm^3/g	Loss of Crystallinity [e] [%]
ETS-4 (f)	1.90	-	312	279	38	0.12	0.00	–
Ni/ETS-4 (i)	1.87	4.86	270	219	56	0.10	0.00	46
Ni/ETS-4 (r)	1.63	4.34	48	4	46	0.00	0.18	100
ETS-10 (f)	2.93	-	386	369	47	0.15	0.00	–
Ni/ETS-10 (i)	2.89	4.88	358	313	49	0.14	0.00	8
Ni/ETS-10 (r)	2.90	4.97	312	222	96	0.10	0.05	23

[a] Determined by EDX analysis considering at least 20 points of investigation for three different magnifications; [b] Valued by BET model; [c] Valued by "t-plot" approach (Harkins–Jura reference equation); [d] Valued as difference of the Vmic by Vtot; [e] Valued as loss of intensity of the main peak respect the fresh sample.

The micropore volumes of the two supports are close to the typical value of other microporous materials, (0.12 and 0.15 cm^3/g for ETS-4 and ETS-10, respectively). The contribution of the internal surface area to the total surface area, for both as-synthesized samples was very important (95% for ETS-10 and 90% for ETS-4). For both samples, the N$_2$ adsorption–desorption technique after the impregnation shows a reduction of the surface area value of ca. 13% for ETS-4 and of ca. 9% for ETS-10. However, all isotherms are of type I (results not shown for briefness); then for both structures, the Ni deposition by impregnation does not significantly affect nor the specific surface area of the final sample neither its microporous volume.

Reduction on Ni/ETS-10 causes a decrease in the internal surface area, i.e., micropore volume, compared with the parent material, whereas the external surface area increases. The N$_2$ adsorption isotherm of Ni/ETS-10 (not shown) after reduction exhibits a hysteresis loop at a relative pressure of 0.45–0.96, which is attributed to the presence of mesopores in the sample. In contrast, Ni/ETS-4 showed a more important loss of internal surface area with respect to the bare ETS-4. This causes an important decrease of the micropore volume of Ni/ETS-4, which is almost zero compared to the parent material. This behavior can be explained by incipient structure collapse, as confirmed by XRD (Figure 1); the collapse of the structure is responsible of the complete loss of the microporous area.

Despite the collapse of crystalline structure, the morphology of ETS-4 is not fully destroyed after the treatments of impregnation and reduction, as shown in Figure 3. The bare sample exhibits a morphology identified as "cuboids", namely an intergrown polycrystalline form wherein small plate crystals grow in tandem to form more complex aggregate shapes [22]. The largest crystal measured approximately 2 μm × 20 μm × 5 μm (a × b × c) for cuboids. The dimensions for the largest individual plates (which make up the cuboids), were less than one-tenth of their intergrown cuboid dimensions. The treatment of impregnation does not modify the morphology of the support, but the reduction treatment promotes a "dissolution" of crystal in agreement with the XRD observations.
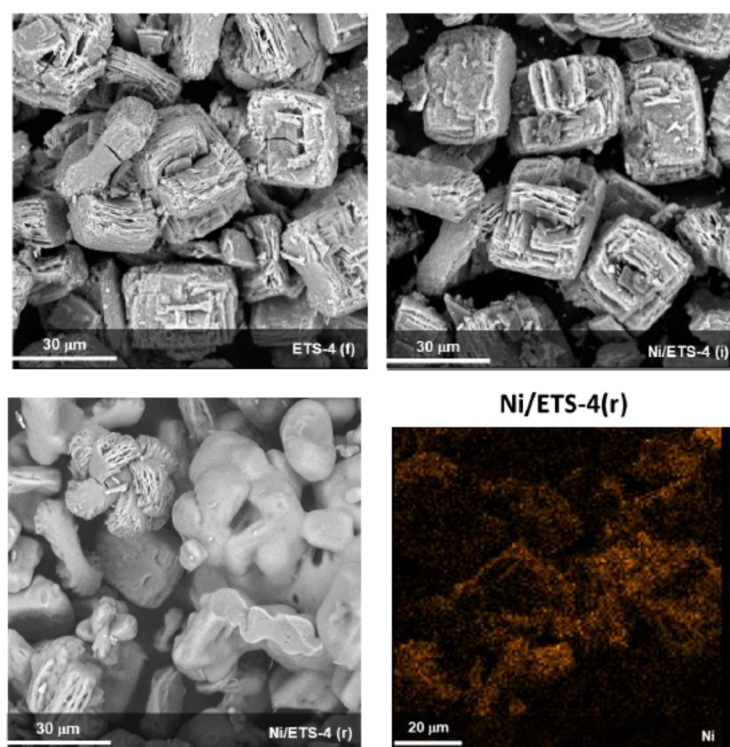
Figure 3. SEM and EDX of bare ETS-4 fresh (f) and Ni/ETS-4 (i) after the impregnation treatment and Ni/ETS-4 (r) after the reduction treatment.

The samples based on ETS-10 support exhibit a cubic shape intergrown morphology with multimodal distribution. The crystal habit is not altered like the ETS-4 based samples by impregnation and reduction step (Figure 4). The distribution of nickel on the ETS-10 surface was regular as mapped by EDX (Figure 4), and metal crystal size was estimated equal to 9.2 nm ($\pm$0.6 nm) through the Debye–Scherrer relation, as elsewhere reported [3].

To study the reducibility of nickel precursor species and the metal–support interaction, TPR-H_2 experiments were performed.

The TPR profiles showed different sets of H_2 consumption peaks, as displayed in Figure 5. However, for both samples, the peaks at lower temperature (367 °C for ETS-4 and 336 °C for ETS-10) can be attributed to the reduction of Ni species located outside of the structure and, therefore, are more easily reducible. In contrast, the peaks located at higher temperature (415 °C for ETS-4 and 392 °C for ETS-10) can be correlated to the nickel species located within the zeolite super cages [23]. These peaks for ETS-4 were shifted to higher temperature with respect to ETS-10: this means a greater interaction of Ni species with the ETS-4 support. At higher temperature, in the TPR profile of ETS-4 a shoulder and broader peak at 500 °C appears, due to the changing of the titanium reduction state from +4 to +3 state [24].

Comparing the TPR-H_2 behavior of nickel-based support of ETS with the other zeolite supports, such as zeolite Y and zeolite Beta [25], it is possible to observe that ETS has a better reducibility of Ni-species, which depends on the low nickel/ETS interactions.

2.2. Catalytic Tests Results

Carbon dioxide methanation was performed over bare ETS supports and Ni/ETS catalysts in the temperature range 300–500 °C. As expected, due to the absence of the active catalytic phase, ETS-4 and ETS-10 supports did not exhibit any catalytic activity, whereas results of Ni based catalysts are reported in the Figure 6. On a dry basis, the only products observed in the outlet gas stream are methane and carbon monoxide.
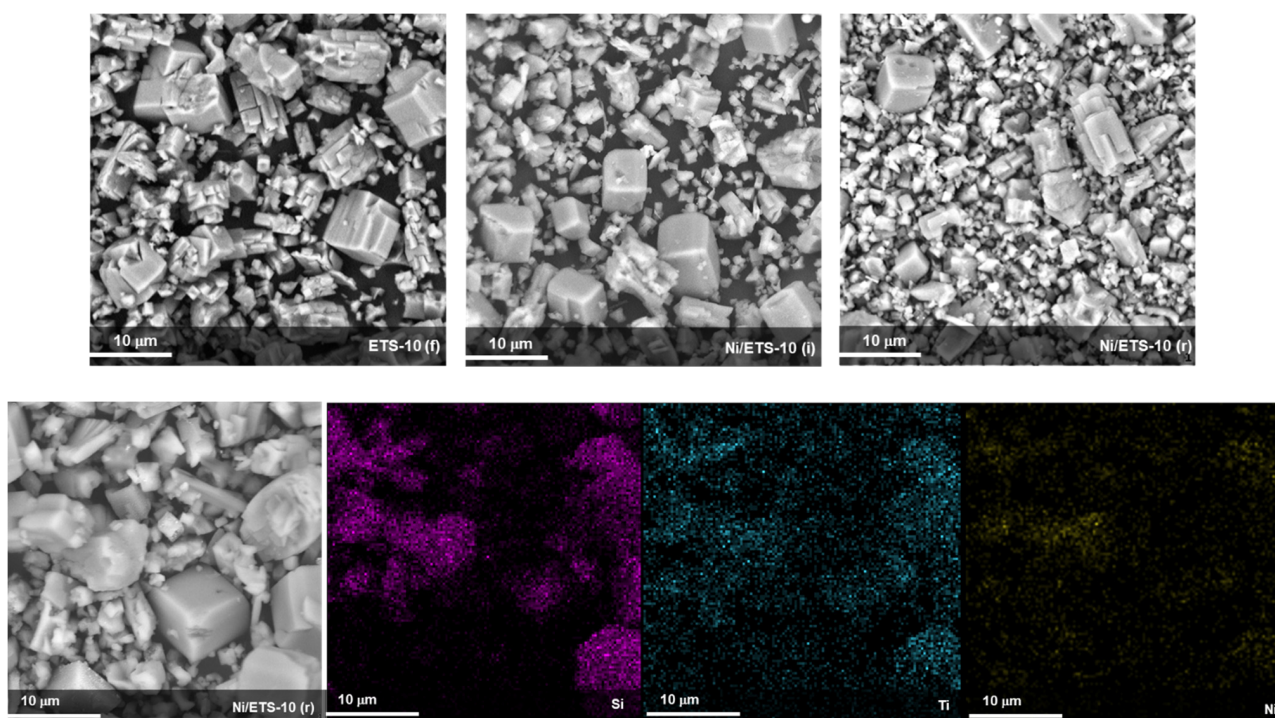
Figure 4. SEM and EDX analysis of bare ETS-10 fresh (f) and Ni/ETS-4 (i) after the impregnation treatment and Ni/ETS-4 (r) after the reduction treatment.
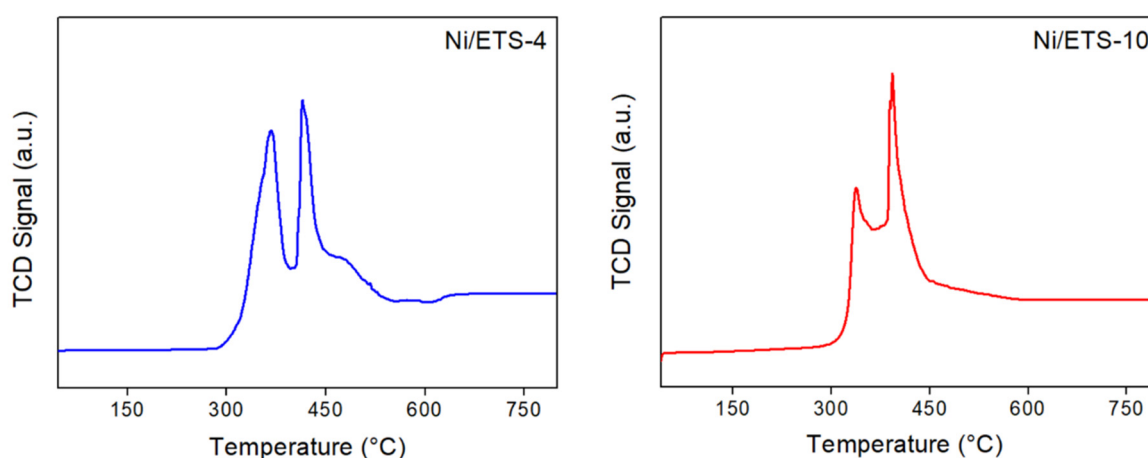

Figure 5. TPR-H_2 profiles of Ni/ETS-4 and Ni/ETS-10 catalysts.

Both catalysts Ni/ETS-4 and Ni/ETS-10 reached optimum conversion at 400 °C, and when the temperature was increased up to 500 °C, the CO_2 and H_2 conversions were reduced due to the thermodynamic limitations of CO_2 methanation. Indeed, the Ni/ETS-4 showed ca. 11% CO_2 conversion at 300 °C, which increased to ca. 62% at 400 °C, and Ni/ETs-10 showed ca. 29% of CO_2 conversion at 300 °C, which increased to ca. 67% at 400 °C, remaining below the thermodynamic limits; this could be due to the greater kinetic barrier for the full reduction of CO_2 (+4) to CH_4 (−4), an eight-electron process that obviously requires high activation energy [26]. Further increase in the reaction temperature at 500 °C led to a slightly decrease in the CO_2 conversion (55% for Ni/ETS-4 and 60% for Ni/ETS-10) due to thermodynamic limit of methanation reaction and to the occurrence of RWGS (reverse water gas shift) reaction [26].
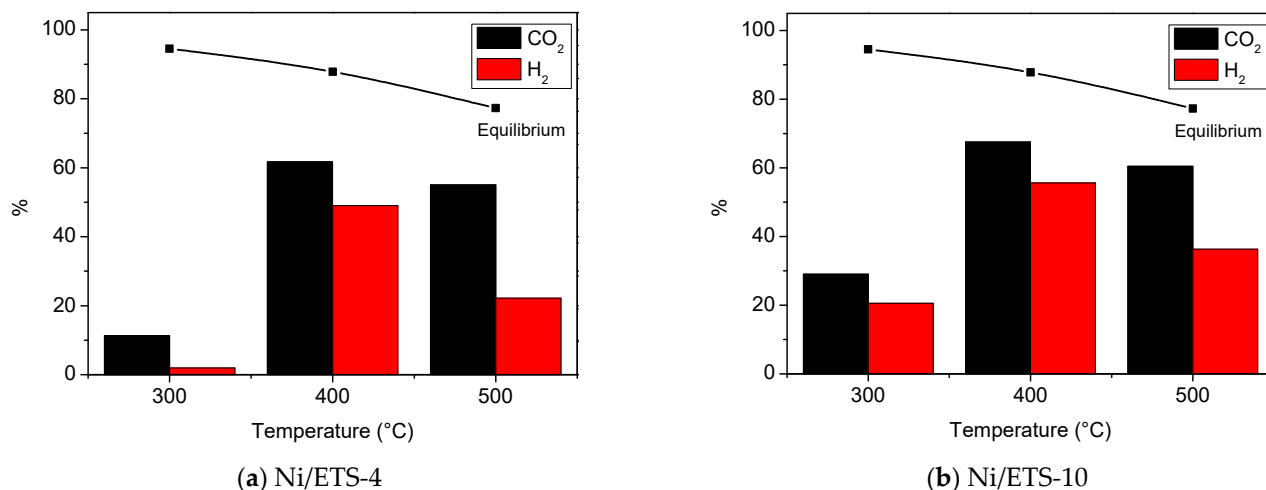
(a) Ni/ETS-4   **(b)** Ni/ETS-10

Figure 6. CO_2 and H_2 conversion of samples Ni/ETS-4 (**a**) and Ni/ETS-10 (**b**) in the temperature range 300–500 °C.

The CH_4 selectivity results are showed in Figure 7. For Ni/ETS-4, the CH_4 selectivity increases from ca. 29% at 300 °C to 42% at 400 °C and then decreases to ca. 2% at 500 °C. In contrast, the CH_4 selectivity increases for Ni/ETS-10 from ca. 56% at 300 °C and to 98% at 400 °C and then decreases to 35.4% at 500 °C (Figure 7). Apparently, this phenomenon was not thermodynamically consistent, because methane concentration should decrease by increasing the temperature, due to the methanation equilibrium; this suggests that the methanation on the Ni/ETS catalysts at relative low temperatures (Tset < 400 °C) was probably a kinetics-controlled reaction [27].
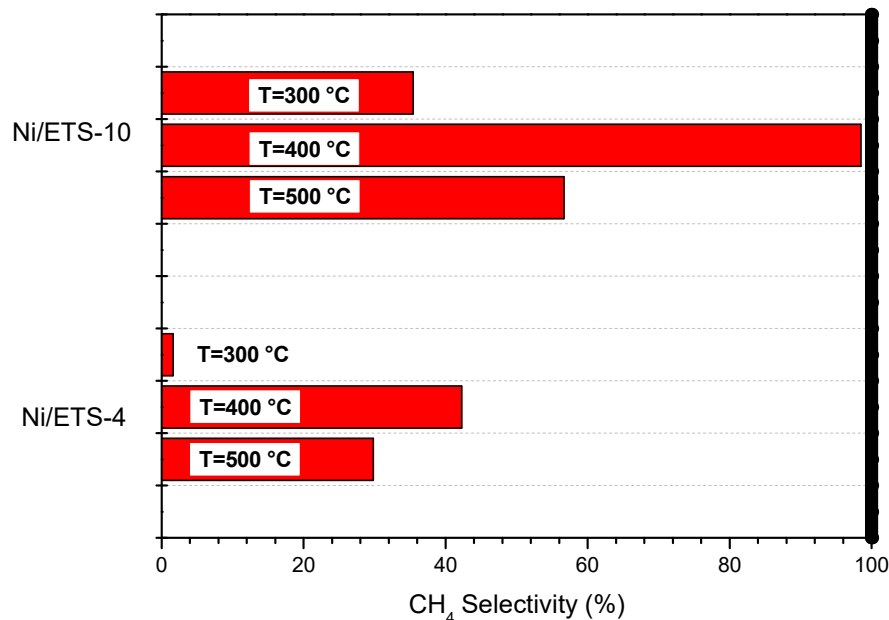

Figure 7. CH_4 selectivity of the Ni/ETS-4 and Ni/ETS-10 catalysts in the temperature range 300–500 °C.

Despite the profiles of CH_4 selectivity for both catalysts are similar, the values of CH_4 selectivity in the range of temperature examined are very different (Figure 7).

Ni/ETS-10 allows obtaining a selectivity value at 400 °C close to 100%; in contrast, at the same temperature, the selectivity of CH_4 reached by Ni/ETS-4 catalyst is lower than the half.

The different behavior of the ETS-4 and ETS-10 can be related to the content of titanium in the framework of the zeolitic structure. The ETS-4 has a higher titanium content that determines the low thermal stability of the impregnated sample, as verified by XRD

diffraction results of the reduced samples (Figure 1). Although the zeolite structure is not preserved, the dispersion of the active metal catalysts is still observed, as indeed confirmed by EDX analysis (Figure 3) and by the high values of conversion. Then, in order to elucidate how the catalytic performance of nickel supported on titanium silicate is affected, the methanation reaction, in the same operative conditions and at the temperature of 400°, has been carried out using silicon dioxide (S 718483 Sigma–Aldrich, S_{BET} 175 m^2/g) and titanium dioxide (637262 Sigma–Aldrich Titanium (IV) oxide, S_{BET} 50 m^2/g) as nickel supports, loading the supports with the same amount of metal. In Figure 8, the comparison of conversion and selectivity values for all supports tested at T = 400 °C are reported. Both supports exhibit a higher value of CO_2 conversion with respect to titanium silicate, but the CH_4 selectivity for Ni catalysts supported on titanium dioxide is consistently lower than all other catalysts. Then, the catalyst based on titanium silicate ETS-4 performs worse value of CH_4 selectivity because it is loaded with higher content of titanium. Moreover, during the reduction procedure, with the collapse of zeolites structure, there is a leaching of titanium from the framework, and at the same time, the titania undergoes a reduction to TiO_x (x < 2). This titanium species covers the nickel particles that, although they remain in their metallic state, are encapsulated by Ti suboxides (TiO_x) after thermal treatment, in agreement with Pan et al. [28]. TiO_x species addresses the CO_2 dissociation, decreases the hydrogen dissociation and then probably causes the change in the selectivity of products [29].
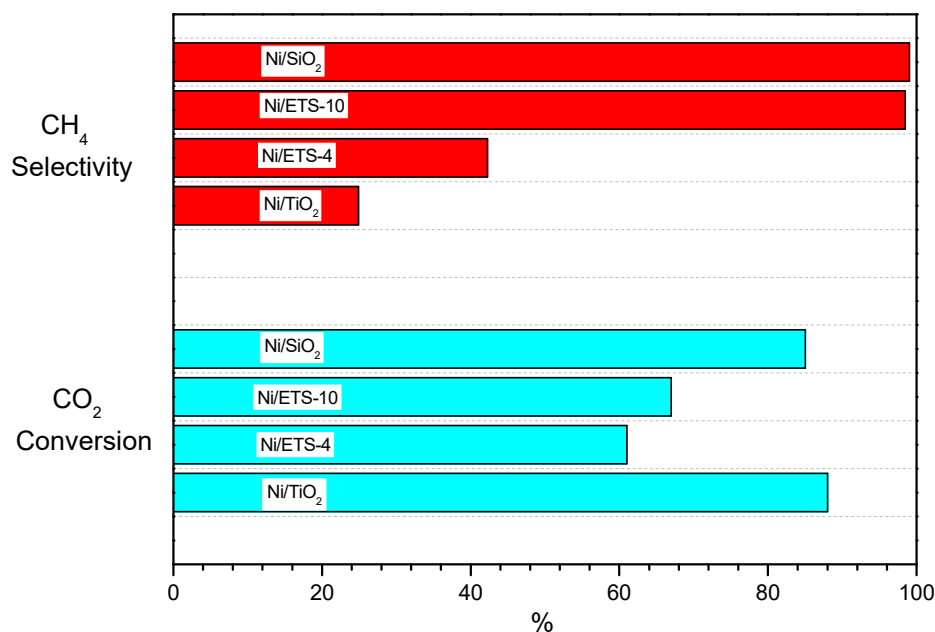

Figure 8. Comparison of different supports for Ni catalysts in the methanation reaction at T = 400 °C and GHSV 30,000 h^{-1}.

Catalysts supported on ETS-10, after reaction, retain the zeolitic structure and the featuring morphology, as showed in the Figure 9. Comparing these results with those obtained by other researcher that used zeolites materials as Ni support for CO_2 methanation in similar reaction conditions, the ETS-10 appears to be a promising support for Ni catalyst in the methanation reaction (Table 2).
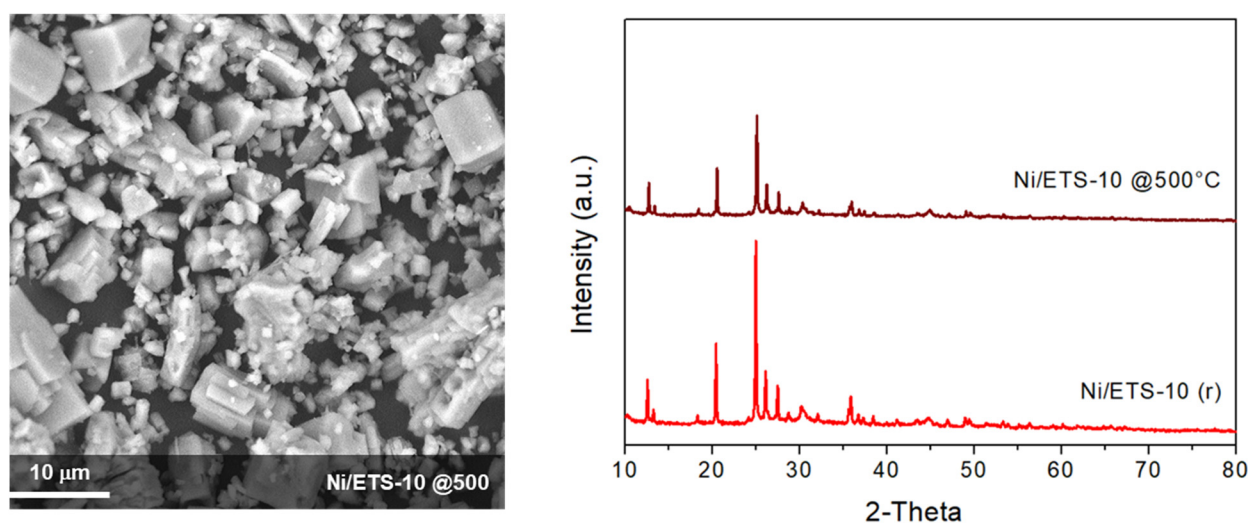
Figure 9. SEM and XRD analysis of Ni/ETS-10 catalyst after reaction at 500 °C.

An interesting comparison can be carried out between Ni catalyst supported on ETS-10 and zeolite Beta is that these supports, in fact, have topological similarities. Both these materials have three-dimensional pore systems, almost identical, although the zeolite Beta is an aluminosilicate composed of tetrahedral SiO_4^{4-} and AlO_4^{5-} units, whereas ETS-10 is a titanosilicate composed of tetrahedral SiO_4^{4-} and octahedral TiO_6^{8-} units [15,30–32].

Comparing the catalytic activity of Ni/ETS-10 and Ni/Beta (Table 2), it was observed that, despite both the lower loading and the higher GHSV employed for Ni/ETS-10, it still exhibits better catalytic activity as compared to Ni/Beta catalyst.

Table 2. Summary of CO_2 methanation performance of Ni/zeolites catalysts at high temperature reaction (T > 350 °C).

Catalyst Composition	H_2/CO_2	GHSV [h^{-1}]	T [°C]	CO_2 Conversion	CH_4 Selectivity	Ref.
5%NiY	4:1	43,000	450	50	95	[23]
5%NiSilicalite	4:1	60,000	450	57	91	[24]
5%Ni/ETS-10	4:1	30,000	400	68	98	[This work]
5%Ni/ETS-10	4:1	30,000	350	52	90	[This work]
10%NiHY	4:1	10,000	350	15	88	[33]
10%NiNaY	4:1	10,000	350	30	82	[33]
10%NiHBeta	4:1	10,000	350	23	82	[33]
10%NiNaBeta	4:1	10,000	350	33	88	[33]
15%NiHbeta	4:1	16,000	350	80	79	[33]
15%NiHbeta	4:1	16,000	400	76	75	[25]

For this material, each TiO_6 unit contributes two minus charges to the framework, leading to the framework oxygen atoms in TiO_6 unit bearing negative charges, regarded as the basic sites [34,35]. For CO_2 adsorption, providing the basic sites on the catalyst surface likely improve CO_2 uptake via acid–base interaction. Further, the CO_2 uptake increases in the presence of oxygen vacancies on the support, ascribed as an adsorption site for CO_2 molecules [36]. Oxygen vacancies can be formed within reducible support (TiO_2, CeO_2, ZrO_2, etc.) since the oxygen vacancy can be mobile inside the lattice and plays an important role in the redox process. The presence of defected sites on Ni/ETS-10 was probably due to the incipient support mesoporosity, indirectly confirmed by the loss of crystallinity introduced after the reduction treatment.

The differences in the catalytic performance between the different Ni-based zeolite supports (Table 2) can be then ascribed to the different zeolite framework, both from a compositional and topological point of view, that influences: (i) the interaction and affinity

with CO_2 and (ii) the metal support interactions, affected by the spatial arrangement and bond angles present in the microporous materials.

3. Experimental Section

3.1. Catalyst Preparation

The two different types of Engelhard Titanium Silicates, namely ETS-4 and ETS-10, were synthesized according to a procedure reported elsewhere [33,37].

Ni catalysts were prepared by the incipient wetness impregnation method. The metal precursor (nickel nitrate hexahydrate $Ni(NO_3)_2 \cdot 6H_2O$ (Sigma–Aldrich, Saint Louis, MO, USA) was opportunely solubilized in an ethanol solution and dispersed over the ETS support, with a total metal content of 5 wt%. After the impregnation process, catalysts were dried at 120 °C for 24 h; subsequently, a mixture of 10 vol% H_2 in He flow was used to reduce catalysts at 500 °C for 2 h, using the same heating and cooling rates. Samples were characterized both after the impregnation/dry process and after the reduction treatment.

3.2. Catalysts Characterization

The identification of phases in fresh, impregnated/dry, reduced and spent catalysts was performed by powder X-ray diffraction (XRD) using a Bruker D2 Phaser using CuKα radiation at 30 kV and 20 mA (Bruker, Karlsruhe, Germany). Peaks attribution was made according with COD (Crystallografic Open Database). The diffraction angles 2θ were varied between 10° and 80° in steps of 0.02° and a count time of 5 s per step.

The reduction of metal oxides was monitored by the temperature programmed reduction (TPR), carried out with a Chemisorb Micromeritics 2750 instrument (Micrometrics, Norcross, GA, USA) under a flux of 50 cm^3 min^{-1} of 10 vol.% H_2/Ar in the temperature range 25–1000 °C at atmospheric pressure.

A Phenom Pro-X scanning electron microscope equipped with an energy-dispersive X-ray (EDX) spectrometer was utilized for SEM analysis (Deben, Suffolk, UK). The EDX analysis was used to evaluate the content and dispersion of metal, acquiring for all samples at least 20 points of investigation at three different magnifications. The counting time for the EDX analysis was 120 s. The results were found to be reproducible to less than ±5% for all samples.

The porous features of the samples were determined by equilibrium adsorption and desorption isotherms of N_2 at 77 K with a Micromeritics ASAP 2020 instrument. Before the analysis, all samples were pre-treated in vacuum condition at 200 °C for 12 h. In order to determine the total surface area of the samples, the data collected were modeled using the BET equation, which is more suitable for solids containing micropores. The evaluation of microporous volumes, internal and external surface area and V–t curves were also interpreted by the "t-plot" method using the Harkins–Jura reference isotherm [38].

3.3. Catalytic Test

CO_2 methanation was carried out in a quartz tubular fixed-bed reactor (1 cm inner diameter, 25 cm length) horizontally placed in a furnace under atmospheric pressure. A mixture gas of H_2/CO_2/N_2 with fixed molar ratio 4/1/1 was fed into the reactor by mass flow controllers (Brooks Instrument, Smart Mass Flow). An Agilent 6890 Plus gas chromatograph equipped with thermal conductivity (TCD) and flame ionization (FID) detectors was used to on-line analyze reactants and products every 20 min. N_2 was used as internal standard for mass balance calibration.

Activity tests (8 h each) were carried at fixed temperature in the range T = 300–500 °C and space velocity GHSV = 30,000 h^{-1}. The total flow rate was 50 cc/min, and GHSV was defined as follows: GHSV = Volumetric flow velocity of gas/ Volume of catalyst.

The CO_2 and H_2 conversion were calculated, on dry basis, by the following formula: X_{CO2} = (moles CO_2 IN – moles CO_2 OUT)/moles CO_2 IN; X_{H2} = (moles H_2 IN – moles H_2 OUT)/moles H_2 IN.

The selectivity of methane was defined as follows: S_{CH4} = moles CH_4 produced/moles of total products.

All reactions were repeated three times, and the deviation measured for the results was $\pm 4\%$. The conversion and selectivity were calculated referring to the stationary values registered when the profile of conversion/selectivity versus time was stable and the phenomenon of deactivation had not occurred yet.

4. Conclusions

The performance of Ni supported on ETS-4 and ETS-10 was investigated. The novel supports were characterized and tested toward the methanation reaction in the range T = 300–500 °C.

The results showed a potential catalytic activity of the Ni/ETS-10 catalyst, characterized by 68% CO_2 conversion and 98% CH_4 selectivity at T = 400 °C.

The ETS-4 was demonstrated to be not a suitable support for the Ni catalyst because of the collapse of the structure, due to the thermal treatment carried out to obtain the catalyst. In addition, the leaching of titanium species had a detrimental effect on the selectivity toward methane.

Ni/ETS-10 retained its framework zeolitic structures and in comparison to other microporous materials exhibited superior catalytic performance.

Author Contributions: Conceptualization, P.F. and A.M.; methodology, P.F., F.M. and P.D.L.; formal analysis, P.F. and A.M.; investigation, M.M. and P.D.L.; data curation, P.F. and M.M.; writing—original draft preparation, P.F. and A.M.; writing—review and editing, M.M. and F.M.; supervision, P.F. All authors have read and agreed to the published version of the manuscript.

Data Availability Statement: Not applicable.

Conflicts of Interest: The authors declare no conflict of interest.

References

1. Malara, A.; Frontera, P.; Antonucci, P.; Macario, A. Smart recycling of carbon oxides: Current status of methanation reaction. *Curr. Opin. Green Sustain. Chem.* **2020**, *26*, 100376. [CrossRef]
2. Frontera, P.; Macario, A.; Malara, A.; Antonucci, V.; Modafferi, V.; Antonucci, P.L. Simultaneous methanation of carbon oxides on nickel-iron catalysts supported on ceria-doped gadolinia. *Catal. Today* **2020**, *357*, 565–572. [CrossRef]
3. Frontera, P.; Malara, A.; Modafferi, V.; Antonucci, V.; Antonucci, P.; Macario, A. Catalytic activity of Ni-Co supported metals in carbon dioxides methanation. *Can. J. Chem. Eng.* **2020**, *98*, 1924–1934. [CrossRef]
4. Frontera, P.; Macario, A.; Malara, A.; Santangelo, S.; Triolo, C.; Crea, F.; Antonucci, P. Trimetallic Ni-Based Catalysts over Gadolinia-Doped Ceria for Green Fuel Production. *Catalysts* **2018**, *8*, 435. [CrossRef]
5. Frontera, P.; Macario, A.; Malara, A.; Modafferi, V.; Mascolo, M.C.; Candamano, S.; Crea, F.; Antonucci, P. CO_2 and CO hydrogenation over Ni-supported materials. *Funct. Mater. Lett.* **2018**, *11*, 1850061. [CrossRef]
6. Busacca, C.; Donato, A.; Faro, M.L.; Malara, A.; Neri, G.; Trocino, S. CO gas sensing performance of electrospun Co_3O_4 nanostructures at low operating temperature. *Sens. Actuators B Chem.* **2020**, *303*, 127193. [CrossRef]
7. Bonaccorsi, L.; Malara, A.; Donato, A.; Donato, N.; Leonardi, S.G.; Neri, G. Effects of UV Irradiation on the Sensing Properties of In_2O_3 for CO Detection at Low Temperature. *Micromachines* **2019**, *10*, 338. [CrossRef] [PubMed]
8. Miceli, M.; Frontera, P.; Macario, A.; Malara, A. Recovery/Reuse of Heterogeneous Supported Spent Catalysts. *Catalysts* **2021**, *11*, 591. [CrossRef]
9. Malara, A.; Paone, E.; Bonaccorsi, L.; Mauriello, F.; Macario, A.; Frontera, P. Pd/Fe_3O_4 Nanofibers for the Catalytic Conversion of Lignin-Derived Benzyl Phenyl Ether under Transfer Hydrogenolysis Conditions. *Catalysts* **2019**, *10*, 20. [CrossRef]
10. Zhang, Q.; Yu, J.; Corma, A. Applications of Zeolites to C1 Chemistry: Recent Advances, Challenges, and Opportunities. *Adv. Mater.* **2020**, *32*, 2002927. [CrossRef]
11. Bonaccorsi, L.; Fotia, A.; Malara, A.; Frontera, P. Advanced Adsorbent Materials for Waste Energy Recovery. *Energies* **2020**, *13*, 4299. [CrossRef]
12. Malara, A.; Frontera, P.; Bonaccorsi, L.; Antonucci, P.L. Hybrid Zeolite SAPO-34 Fibres Made by Electrospinning. *Materials* **2018**, *11*, 2555. [CrossRef] [PubMed]

13. Bacariza, M.C.; Graça, I.; Lopes, J.; Henriques, C. Tuning Zeolite Properties towards CO_2 Methanation: An Overview. *ChemCatChem* **2019**, *11*, 2388–2400. [CrossRef]

14. Rocha, J.; Anderson, M. Microporous Titanosilicates and other Novel Mixed Octahedral-Tetrahedral Framework Oxides. *Eur. J. Inorg. Chem.* **2000**, *5*, 801–818. [CrossRef]

15. Anderson, M.; Terasaki, O.; Ohsuna, T.; Malley, P.J.O.; Philippou, A.; Mackay, S.P.; Ferreira, A.; Rocha, J.; Lidin, S. Microporous titanosilicate ETS-10: A structural survey. *Philos. Mag. B* **1995**, *71*, 813–841. [CrossRef]

16. Faroldi, B.; Lombardo, E.; Cornaglia, L.; Irusta, S. Application of ETS-10 microporous titanosilicate as support of Ru nanoparticles for hydrogen production. *Appl. Catal. A Gen.* **2012**, *417-418*, 43–52. [CrossRef]

17. Philippou, A.; Naderi, M.; Pervaiz, N.; Rocha, J.; Anderson, M. n-Hexane Reforming Reactions over Basic Pt-ETS-10 and Pt-ETAS-10. *J. Catal.* **1998**, *178*, 174–181. [CrossRef]

18. Fu, W.; Yin, C.; Feng, Y.; Zhang, L.; Cheng, F.; Fang, Z.; Zhu, C.; Tang, T. Synergistic catalysis of the Brönsted acid and highly dispersed Cu on the mesoporous Beta zeolite in the intermolecular aminoazidation of styrene. *Appl. Catal. A Gen.* **2021**, *609*, 117907. [CrossRef]

19. Sebastian, V.; Irusta, S.; Mallada, R.; Santamaria, J. Selective oxidation of CO in the presence of H_2, CO_2 and H_2O, on different zeolite-supported Pt catalysts. *Appl. Catal. A Gen.* **2009**, *366*, 242–251. [CrossRef]

20. Cruciani, G.; De Luca, P.; Nastro, A.; Pattison, P. Rietveld refinement of the zorite structure of ETS-4 molecular sieves. *Microporous Mesoporous Mater.* **1998**, *21*, 143–153. [CrossRef]

21. Vosoughi, M.; Maghsoudi, H.; Gharedaghi, S. Ion-exchanged ETS-10 adsorbents for CO_2/CH_4 separation: IAST assisted comparison of performance with other zeolites. *J. Nat. Gas Sci. Eng.* **2021**, *88*, 103862. [CrossRef]

22. Mintova, S.; Stein, B.; Reder, J.M.; Bein, T.; Galarneau, A.; Di Renzo, F.; Fajula, F.; Vedrine, J. Zeolites and Mesoporous Materials at the Dawn of the 21st Century. In Proceedings of the 13th International Zeolite Conference, Montpellier, France, 8–13 June 2001.

23. Wei, L.; Haije, W.; Kumar, N.; Peltonen, J.; Peurla, M.; Grenman, H.; de Jong, W. Influence of nickel precursors on the properties and performance of Ni impregnated zeolite 5A and 13X catalysts in CO2 methanation. *Catal. Today* **2021**, *362*, 35–46. [CrossRef]

24. Bal, R.; Chaudhari, K.; Srinivas, D.; Sivasanker, S.; Ratnasamy, P. Redox and catalytic chemistry of Ti in titanosilicate molecular sieves: An EPR investigation. *J. Mol. Catal. A Chem.* **2000**, *162*, 199–207. [CrossRef]

25. Quindimil, A.; De-La-Torre, U.; Pereda-Ayo, B.; Marcos, J.A.G.; González-Velasco, J.R. Ni catalysts with La as promoter supported over Y- and BETA- zeolites for CO_2 methanation. *Appl. Catal. B Environ.* **2018**, *238*, 393–403. [CrossRef]

26. Xu, L.; Yang, H.; Chen, M.; Wang, F.; Nie, D.; Qi, L.; Lian, X.; Chen, H.; Wu, M. CO_2 methanation over Ca doped ordered mesoporous Ni-Al composite oxide catalysts: The promoting effect of basic modifier. *J. CO_2 Util.* **2017**, *21*, 200–210. [CrossRef]

27. Lu, H.; Yang, X.; Gao, G.; Wang, J.; Han, C.; Liang, X.; Li, C.; Li, Y.; Zhang, W.; Chen, X. Metal (Fe, Co, Ce or La) doped nickel catalyst supported on ZrO_2 modified mesoporous clays for CO and CO_2 methanation. *Fuel* **2016**, *183*, 335–344. [CrossRef]

28. Pan, J.-M.; Madey, T.E. The encapsulation of Fe on $TiO_2(110)$. *Catal. Lett.* **1993**, *20*, 269–274. [CrossRef]

29. van de Loosdrecht, J.; van der Kraan, A.M.; van Dillen, A.J.; Geus, J.W. Metal-Support Interaction: Titania-Supported and Silica-Supported Nickel Catalysts. *J. Catal.* **1997**, *170*, 217–226. [CrossRef]

30. Aziz, M.; Jalil, A.; Triwahyono, S.; Mukti, R.; Taufiq-Yap, Y.; Sazegar, M. Highly active Ni-promoted mesostructured silica nanoparticles for CO_2 methanation. *Appl. Catal. B Environ.* **2014**, *147*, 359–368. [CrossRef]

31. Goodarzi, F.; Kang, L.; Wang, F.R.; Joensen, F.; Kegnaes, S.; Mielby, J. Methanation of Carbon Dioxide over Zeolite-Encapsulated Nickel Nanoparticles. *ChemCatChem* **2018**, *10*, 1566–1570. [CrossRef]

32. Liang, C.; Zhang, L.; Zheng, Y.; Zhang, S.; Liu, Q.; Gao, G.; Dong, D.; Wang, Y.; Xu, L.; Hu, X. Methanation of CO_2 over nickel catalysts: Impacts of acidic/basic sites on formation of the reaction intermediates. *Fuel* **2020**, *262*, 116521. [CrossRef]

33. Vuono, D.; Guzzo, M.; De Luca, P.; Nagy, J.B. Physico-chemical characterisation of zirconium-based self-bonded ETS-4 pellets. *J. Therm. Anal. Calorim.* **2013**, *116*, 169–182. [CrossRef]

34. Tang, T.; Zhang, L.; Fu, W.; Ma, Y.; Xu, J.; Jiang, J.; Fang, G.; Xiao, F.-S. Design and Synthesis of Metal Sulfide Catalysts Supported on Zeolite Nanofiber Bundles with Unprecedented Hydrodesulfurization Activities. *J. Am. Chem. Soc.* **2013**, *135*, 11437–11440. [CrossRef]

35. Yu, Q.; Zhang, L.; Guo, R.; Sun, J.; Fu, W.; Tang, T.; Tang, T. Catalytic performance of CoMo catalysts supported on mesoporous ZSM-5 zeolite-alumina composites in the hydrodesulfurization of 4,6-dimethyldibenzothiophene. *Fuel Process. Technol.* **2017**, *159*, 76–87. [CrossRef]

36. Varilla, L.A.A.; Seriani, N.; Montoya, J.A. Molecular adsorption and dissociation of CO_2 on TiO_2 anatase (001) activated by oxygen vacancies. *J. Mol. Model.* **2019**, *25*, 1–8. [CrossRef] [PubMed]

37. De Luca, P.; Mastroianni, C.; Siciliano, C.; Nagy, J.B.; Macario, A. Preparation of ETS-10 Microporous Phase Pellets with Color Change Properties. *Gels* **2019**, *5*, 42. [CrossRef]

38. Gregg, S.J.; Sing, K.S.W. *Adsorption, Surface Area and Porosity*; Academic Press: London, UK, 1991.